Atmos. Chem. Phys. Discuss., https://doi.org/10.5194/acp-2019-308
Manuscript under review for journal Atmos. Chem. Phys.
Discussion started: 23 May 2019

Atmospheric Chemistry and Physics Discussions

Measurement of aerosol properties during wintertime in Beijing

Misti Levy Zamora[1,3], Jianfei Peng[1,2], Min Hu[2,*], Song Guo[1,2], Wilmarie Marrero-Ortiz[1], Dongjie Shang[2], Jing Zheng[2], Zhuofei Du[2], Zhijun Wu[2] & Renyi Zhang[1,2,*]

[1]Department of Atmospheric Sciences and Department of Chemistry, Center for Atmospheric Chemistry and the Environment, Texas A&M University, College Station, TX 77843, USA

[2]State Key Joint Laboratory of Environmental Simulation and Pollution Control, College of Environmental Sciences and Engineering, Peking University, Beijing 100871, China

[3]Department of Environmental Health and Engineering, Johns Hopkins Bloomberg School of Public Health, 615 N. Wolfe St., Baltimore, Maryland 21205, USA

Correspondence to: Min Hu (minhu@pku.edu.cn); Renyi Zhang (Renyi-Zhang@tamu.edu)

Abstract. Severe haze events with exceedingly high-levels of aerosols have occurred frequently in China in recent years, threatening human health and affecting regional and global radiative budget. A better knowledge of aerosol properties during haze events, particularly for those occurring during wintertime, will be helpful for elucidating the haze formation mechanism. In this study, we conducted a field measurement at an urban site in Beijing during January and February of 2015. A suite of aerosol instruments was deployed to measure a comprehensive set of aerosol chemical and physical properties. The haze events in winter, regulated by meteorological conditions, typically start with a new particle formation event and progress in terms of the subsequently continuous growth of the nucleation mode particles to submicron particles over the following multiple days. Particulate organic matters are primarily responsible for producing the nucleation mode particles, while secondary organic and inorganic components jointly contribute to the high aerosol mass observed during haze events. The average effective density and kappa value of ambient particles are approximately 1.37 g cm^{-3} and 0.25 during the clean days, and 1.42 g cm^{-3} and 0.4 during the severe haze episodes, respectively, indicating the formation of secondary inorganic species during the development of the severe haze events. Our results reveal that the periodic cycles of severe haze formation in Beijing during wintertime are attributed to the fast secondary aerosol formation due to the high gaseous precursor concentrations and the stagnant air mass, which are analogous to the severe haze events observed during autumn.

1 introduction

Three decades of rapid industrialization have made China the second largest economy in the world and the "World's Factory". This rapid economic development has resulted in a deterioration of the quality of air, water, land, and ecosystems (Chang et al., 2009; Su et al., 2012; Wang et al., 2008; WHO et al., 2006). One of the most substantial environmental issues is the severe haze events caused by the elevated mass concentration of fine particulate matter ($PM_{2.5}$) that frequently occurred in many regions of China.

Atmos. Chem. Phys. Discuss., https://doi.org/10.5194/acp-2019-308
Manuscript under review for journal Atmos. Chem. Phys.
Discussion started: 23 May 2019

Atmospheric Chemistry and Physics Discussions

$PM_{2.5}$ is mainly composed of sulfate, nitrate, ammonium, organics, and elemental carbon in China (Zheng et al., 2016). To elucidate the mechanism of severe $PM_{2.5}$ pollution, considerable efforts have been made in the past few years. Huang et al. (2014) demonstrated that severe $PM_{2.5}$ pollution in four megacities in China, i.e., Beijing, Shanghai, Guangzhou, and Xi'an), was driven to a large extent by the secondary aerosol formation. Guo et al. (2014) elucidated that the formation of severe urban haze in Beijing during autumn could be characterized by two distinct aerosol formation processes: 1) the nucleation of aerosols and 2) the subsequent growth of these aerosols driven by secondary formation. The transition from a clean period to a polluted period can be remarkably fast (Guo et al., 2014). Wang et al. (2016) further proposed that aqueous-phase reaction could be of great importance for the secondary aerosol formation during severe haze stage. Moreover, some other studies also reveal key interactions between haze formation with meteorological conditions, such as humidity and planetary boundary layer (PBL) (Ding et al., 2016; Tie et al., 2017).

Aerosol properties can provide essential information on the primary emission sources and the atmospheric evolution of atmospheric aerosols. For example, particle hygroscopicity is a key factor in identifying the species of ambient aerosols and the changes aerosols undergo during the aging process (Chang et al., 2010; Guo et al., 2014). The hygroscopicity of ambient aerosols can be quantified by using the parameter kappa (κ) or the hygroscopic growth factor (HGF) (Petters and Kreidenweis, 2007). Particle effective density is also a key parameter to probe primary combustion emission and the aging of primary soot aerosols (Peng et al., 2016). Several measurements have previously investigated the particle density in Beijing via several filter-based methods (Hu et al., 2012; Yue et al., 2010), with a time resolution of about half a day. Few measurements have provided high time-resolution and size-resolved density information (Guo et al., 2014; Qiao et al., 2016), hindering the in-depth investigation of atmospheric aging processes. In addition, most of the previous observational studies focused on the aerosol properties and haze formation in Beijing have been carried out in summer and autumn (Guo et al., 2014; Huang et al., 2010; Sun et al., 2014). As the most severe haze episodes often occur during wintertime, more observation on aerosol properties in winter will be helpful for investigating the severe haze formation mechanism (Hu et al., 2016; Sun et al., 2013).

In this study, a field campaign was conducted to measure ambient particulate matter and gaseous concentration in Beijing from January to February 2015 to better understand the haze formation mechanism during wintertime in Beijing. The physical and chemical properties of ambient aerosols during different pollution stages, including particle size distributions, size-resolved effective density measurements, and chemical composition, were simultaneously measured during the campaign. The contribution of secondary aerosol formation to the $PM_{2.5}$ mass concentration in Beijing was evaluated according to ambient gas concentrations and aerosol properties. Furthermore, the pollution features observed during winter and autumn were further compared to understand how the haze formation mechanisms in different seasons.

2 Methodology and Instrumentation

All measurements were conducted at PeKing University urban atmosphere Environment monitoRing Station (PKUERS, 39°59'21" N, 116°18'25' E) located in the northwestern Beijing urban area. The site is located outside the fourth-ring road with no significant stationary sources or mobile sources within 200 m and is likely representative of the Beijing urban area

(Wu et al., 2008). The instruments were located in an air-conditioned room on the roof of a building about 15 m above ground level. A suite of state-of-the-art instruments was deployed to simultaneously measure the gaseous species and aerosol properties, including particle mass concentration, size distribution, chemical composition, and size-resolved effective density and hygroscopicity.

A Tapered Element Oscillating Microbalance (TEOM, 1400a, Thermo, USA.) with a $PM_{2.5}$ cyclone inlet was used to measure the ambient $PM_{2.5}$ mass concentration. The sampling flow was 16.7 LPM, of which 1 LPM was introduced to the instrument. The TEOM measures the mass collected on a filter by monitoring the corresponding frequency changes of a tapered element. As the mass concentration increased on the replaceable filter, the tube's natural frequency of oscillation decreased. The mass concentration was determined from the change in the oscillation frequency.

An Aerodyne High-Resolution Time-of-Flight Aerosol Mass Spectrometer (HR-ToF-AMS) was employed to measure the size-resolved chemical compositions of submicron particles (Hu et al., 2016). The HR-ToF-AMS operated in 5-minute cycles, including a V-mode to obtain the mass concentrations of non-refractory species such as ammonium, sulfate, nitrate, organics, and chloride, a W-mode to obtain high-resolution mass spectral data, and a particle time-of-flight mode to determine size distributions of species measured with the V-mode. The HR-ToF-AMS was calibrated for inlet flow, ionization efficiency, and particle size at the beginning, middle, and end of the measurements (Hu et al., 2016). The calibration of ionization efficiency was conducted with size-selected pure ammonium nitrate particles. The detection limit was defined as three times the standard deviations of the observed signals. The detection limits of sulfate, nitrate, ammonium, chloride, and organics were determined to be 0.008, 0.004, 0.026, 0.004, and 0.033 μg m^{-3}, respectively.

A scanning mobility particle sizer (SMPS) and a nano-SMPS were used to concurrently measure the number size distribution of particles between 3 nm and 600 nm in the ambient air (Wang et al., 2013). Ambient aerosols were sampled at a rate of 16.7 LPM through a 3 m long thermally insulated 1/2" stainless steel tube. Before being measured by the SMPS and nano-SMPS, an airflow of 1.8 LPM passed through a series of Nafion driers (Perma Pure, Inc.) to reduce the relative humidity of the aerosols to less than 30 %. In the SMPS/nano-SMPS system, polydisperse aerosols were brought to charge equilibrium and passed through the DMA and CPC to determine the particle size and concentration. The sheath flow rate was maintained at 3 LPM for the DMA and 15 LPM for nano-DMA. The particle size was calibrated with mono-disperse polystyrene latex spheres (PSL, Duke Scientific, Palo Alto, California, USA.) with nominal diameters of 100 - 500 nm.

A combination DMA-Aerosol Particle Mass analyzer (APM, model 3600, Kanomax Inc., Japan) system was employed to measure the particle size-resolved density. Ambient airflow first passed through a DMA, where the voltage was fixed to provide continuous monodisperse particles. Then, the monodisperse aerosol flow passed through an APM, where the particle mass distribution could be obtained. Effective density is defined as the measured mass over the volume where the particle is assumed to be a sphere based on the measured particle size; therefore, compounds with the same mass but different shapes may have extremely different effective densities. The effective densities for five-particle sizes were obtained hourly. Since the mobility diameter corresponds to a unique voltage, if the applied voltage and effective density of PSL are known, the effective density of the sample aerosols can be calculated by the following equation,

Atmos. Chem. Phys. Discuss., https://doi.org/10.5194/acp-2019-308
Manuscript under review for journal Atmos. Chem. Phys.
Discussion started: 23 May 2019

$$\rho_{eff} = {}^{V_{APM}}/_{V_{APM,PSL}} \times \rho_{PSL} \quad (1)$$

where V_{APM} and $V_{APM,\ PSL}$ are the fitted peak voltages in APM corresponding to the masses of sample and PSL particles, respectively. The material density of the PSL particles is 1.054 g cm^{-3}. Each effective density distribution scans from 0.1 to 2.2 g cm^{-3}. Effective density peaks at 1.76, 1.78, and 1.73 g cm^{-3} correspond to ammonium sulfate, ammonium bisulfate, and ammonium nitrate, respectively. The effective density of organic aerosols can vary significantly due to the numerous compounds in this category, the different emission sources, and the distinct structures of the compounds. Turpin and Lim (2001) reported that the density of secondary organic aerosols from the oxidation of aromatics and alkanes was between 1.20 and 1.40 g cm^{-3}. The effective densities of fresh black carbon (BC), mineral dust, and sea salt were found to be 0.1 - 0.6, 2.65, and 2.2 g cm^{-3}, respectively (Geller et al., 2006; Khalizov et al., 2009). This methodology has been utilized and discussed previously (Levy et al., 2014).

The hygroscopicity of ambient aerosols was parameterized by the kappa (κ), which is derived using the following formula (Petters and Kreidenweis, 2007),

$$\kappa = \frac{\nu \rho_d}{\rho_w} \frac{M_w}{M_d} = \sum_i \varepsilon_i \kappa_i \quad (2)$$

where M, ρ, ν, and ε, are the molecular weight, molecular densities, van Hoff factor, and volume fraction of the component in the aerosols mass, respectively. Using the volume-weighted average fraction determined by the AMS measurement and the ε_i values of 0.0, 0.09, 0.48, 0.58, 0.55, and 0.246 for BC, organic aerosols, SO_4^{2-}, NO_3^-, NH_4^+, and Cl^-, respectively, the chemical composition derived kappa was calculated.

The PBL was determined by utilizing the National Oceanic and Atmospheric Administration's (NOAA) hybrid single-particle Lagrangian integrated trajectory (HYSPLIT) model.

3 Results and Discussion

3.1 Observed haze cycles

Four PM pollution cycles were documented during the measurement in 2015 winter (Fig. S1). Frequently, the large-scale meteorology governed the length and severity of haze events due to the periodical occurrence of exceedingly stagnant airmass and strong, cleansing winds. During the observation period, low $PM_{2.5}$ concentration was accomplished with the strong northerly wind. While the episodes with the highest $PM_{2.5}$ concentration (i.e., 22 January and 26 January) exhibited calm winds and low PBL heights (Fig. S1), which trapped primary emission near their sources and secondary pollutants within the formation area. Temporal evolutions of the particle mass and number concentration, chemical composition, and size distribution and the average diameter of the first and second pollution cycles (between 21 and 27 January 2015) are illustrated in Figure 1. The first haze event began with an NPF event, which was followed by the continuous particle growth over three

days (Fig. 1A). On the clean days (i.e., 21 January and 27 January) the strong wind and the high PBL diluted the pollutants both vertically and horizontally (Fig. S1). The total number concentration exceeded 300,000 cm^{-3} during the NPF event, but generally decreased after the NPF event and remained around 100,000 cm^{-3} (Fig. 1C). The average diameter of all ambient particles was only about 10 nm during the NPF event and steadily increased until their average diameter was near 150 nm (Fig. 1D). During nighttime of 22 January, the particle mass concentration increased but the diameter decreased, which is possibly due to the combination of the primary emission of smaller particles and the compressed PBL during nighttime. Minor mass growth was observed on 21 January (Fig. 1B), with an increase from 8 to 30 μg m^{-3}. The most rapid mass concentration increase occurred on 22 January, with an increase from 30 to 300 μg m^{-3}.

During the early morning of January 24, a weak front passed through the sampling site, which led to weak winds from the north and increased PBL to around 700 m (Fig. S1), diluting the ambient $PM_{2.5}$ concentration (to about 30 μg m^{-3} on average in the daytime on January 24). Meanwhile, a large amount of primary emission in the morning rush hour lowered the average particle diameter to smaller than 50 nm. After the frontal passage, the winds shifted to southerly, which recirculated the polluted air mass back to the sampling site. Though the mass concentration exhibited two distinguish pollution cycles, the air mass of this event as a whole was likely the same. On 25 January, weak southerly winds continued, and the boundary layer height decreased to about 300 m. The stagnant conditions led to a rapid accumulation of pollutants. The total number and mass concentrations of ambient $PM_{2.5}$ gradually grew to 130 nm and 250 μg m^{-3} in the following two days, respectively (Fig. 1B, 1D). Meanwhile, the aerosol constituents generally remained similar during this episode (Fig. 1B).

3.2 Aerosol chemical composition, hygroscopicity, and density

Organic aerosols accounted for the largest percentage of the aerosol mass during both the clean (58%, 21 January) and the polluted phase (52%, 23 January). Nitrate, ammonium, and sulfate accounted for 12%, 12%, and 16%, respectively, during the clean phase, and remained relatively constant at 20%, 14%, and 12%, respectively, throughout the polluted period of the first and the second cycles. The contribution of chloride to PM remained constant at about 2%.

The average kappa values of ambient between 21 January and 29 January 2015 are shown in Figure 3A. Both the diurnal cycles and the overall trend governed by the pollution cycle are evident in the aerosol hygroscopicity. Diurnally, the least hygroscopic aerosols occurred overnight, while the most hygroscopic aerosols were found near sunset. The reduced nighttime hygroscopicity was concurrently observed with the transiently elevated organic aerosol mass concentration (Fig. 1) and reduced effective density of the larger particles (Fig. 3B), which may be due to the increase of vehicle emissions of primary organic aerosols and black carbon in the city overnight. The increased hygroscopicity in the mid-morning and early afternoon hours (9 a.m. to 1 p.m.) was due to the rapid increase in the mass concentrations of nitrate, ammonium, and sulfate aerosols (Fig. 1B), consistent with previous studies in Mexico City which showed that ammonium nitrate rapidly formed in the morning (Hennigan et al., 2008). From the onset of the first pollution cycle on 21 January to the morning of 25 January, the kappa value increased from 0.15 to 0.42.

The effective densities for 81, 97, 151, and 240 nm particles are exhibited in Figure 3B. During the clean phase (e.g., 22 January), all four particle sizes exhibited effective density values that clustered near 1.37 g cm^{-3}. However, as the haze event developed, the effective densities of particles with the four sizes became increasingly differentiated. When the $PM_{2.5}$ mass concentration decreased at the end of the haze event (i.e., 27 January), the effective density of the particles again clustered near 1.36 g cm^{-3}. The lower average effective density during the clean period can be attributable to the organic dominated aerosol composition as well as the fresh low-density BC emission. Furthermore, the increasing effective density corresponds to the increasing sulfate and nitrate composition that was observed as the haze events progressed (Fig. 1B). Generally, the effective density distributions were unimodal, indicating that the aerosols were internally mixed. The weighted average density, i.e., the effective density weighted by the total number concentration of particles near each size of the four particles sizes, increased throughout the haze event, but this was primarily due to the changes in the particles smaller than 100 nm. The effective density of smaller particles (i.e., 81 and 97 nm) increased as the ambient atmosphere became more polluted, whereas the densities of larger particles (i.e., 151 and 240 nm) remained near 1.37 g cm^{-3}. Figure 4 shows the diurnal variation of the effective densities of 81, 97, 151, and 240 nm particles during the entire observational campaign as well as the polluted period and the clean period. An evident diurnal variation of effective density was observed, i.e., higher density overnight, lower density during the morning and evening rush hours, and moderately stable density during the daytime. Over the entire campaign, the lowest density was observed after the evening rush hour (i.e., 1.38 g cm^{-3} for 81 nm particles), and the highest density (~ 1.41 g cm^{-3} for 81 nm particles) was observed in the early morning before the intensification of heavy traffic. During the high traffic periods (i.e., 6 - 9 a.m. and 4 - 8 p.m.), the decreasing effective density was likely due to the increasing concentrations of BC and primary organic aerosols (POA). Overnight, the effective density increased due to the formation of inorganic species on aerosols. The variations in the effective density were suppressed during the polluted days. This may be because the newly emitted particles were being mixed into a relatively higher concentration of particles. Therefore, the average effective density of the entire air mass was not as sensitive to the primary emitted particles during rush hours.

3.3 Comparisons of aerosol properties in autumn and winter

In Figure 5, a comparison of the mass concentration, total number concentration, and the average diameter of ambient particles from representative pollution cycles from the autumn 2013 and winter 2015 field campaigns are displayed (Guo et al., 2014). The chemical composition during the clean and polluted period from both campaigns is also exhibited in Figure 2. Both seasonal haze events began with NPF events, which were typically followed by particle growth over several days. Overall various properties (i.e., particle size, number concentration, chemical composition, and hygroscopicity) appear to be similar in the autumn and winter campaigns, with a few notable caveats.

The particle growth and formation were more efficient in the autumn campaign: i.e., the NPF events resulted in a higher total number concentration in the autumn, and the final average particle diameter was near 180 nm compared to 150 nm in the winter, which may be attributable to the stronger solar irradiation in autumn than in winter. Furthermore, if the mixing layer

depth is taken into consideration (Fig. S1), the particle growth and the secondary aerosol formation were likely much more efficient in the autumn because while the resultant concentrations were similar, the mixing layer was nearly twice as high during autumn compared that during winter. Organics were the dominated aerosols species during clean episodes in both autumn and winter at 79 and 58%, respectively (Fig. 2), while inorganic species, i.e., sulfate, nitrate, and ammonium, were more abundant in the polluted episodes in both campaigns. More organic aerosols were observed in the winter polluted episode, likely due to the increased POA emissions from residential heating during winter. The trends in the hygroscopicity of the particles are similar between the two seasons, with the only significant differences occurring on the clean days (i.e., 21 January, 25 September, 27 January, and 1 October). The hygroscopicity of the autumn aerosols (25 September) during the clean phase was much lower (0.2) than the hygroscopicity of the wintertime aerosols (0.35). This is likely due to the higher proportion of sulfate in PM during the winter (7% in the autumn, 16% in the winter) due to residential heating and suppressed dilution of local pollutant (mixing layer depth of 1100 m compared to 2200 m, Fig. S1.).

4 Conclusions and implication

We have elucidated the influence of meteorology, local emissions, and aerosol processes on severe haze events in Beijing during winter by conducting comprehensive aerosol properties measurements. Formation of severe haze in Beijing is comprised of two distinct processes of secondary aerosol formation, i.e., the nucleation that initially produces high concentrations of nanoparticles and the subsequent continuous growth from the nucleation mode particles to submicron particles. Our analysis of the aerosol chemical compositions suggests that organic aerosols are primarily responsible for producing the nucleation mode particles, while secondary organic aerosols and inorganic salts contribute jointly to the particle growth. The combination of the high aerosol nucleation potential and efficient subsequent growth over several days uniquely differentiates the severe $PM_{2.5}$ episodes in Beijing from those typically observed in other regions worldwide. We show that the periodic cycles of haze episodes during the autumn and winter seasons in Beijing are closely linked to the meteorological conditions. During haze events, stagnant air masses typically develop under the calm or weak southerly wind, which traps the local pollutants.

From the perspective of pollution control, it may be feasible to suppress the aerosol growth processes to reduce the $PM_{2.5}$ levels in Beijing. Our results imply that an effort to solely control emissions of primary particles would result in only a minor reduction of the $PM_{2.5}$ mass concentration, while the reductions in the emissions of the aerosol precursor gases, i.e., VOCs and NO_X from local transportation and SO_2 from regional industrial sources, are critical for remediation of the haze pollution in Beijing. Such a viewpoint of severe haze formation is critical for improving formulating effective regulatory policies by decision-makers at the central and local government levels.

Data availability. The data set is available upon request by contacting Renyi Zhang (Renyi-Zhang@tamu.edu).

Author contributions. M.H., S.G., Z.W. and R.Z. organized the field campaign. M.L.Z., J.P., W.M., D.S., J.Z., and Z.D. conducted the online measurement and analyzed the data. M.L.Z. and J.P. wrote the paper with input from R.Z. All authors contributed to the discussion on the results. M.L.Z. and J.P. contribute to this paper equally.

Competing interests. The authors declare that they have no conflict of interest.

Acknowledgments. The paper is funded by National Natural Science Foundation of China (91544214,91844301); National research program for key issues in air pollution control (DQGG0103); National Key Research and Development Program of China (2016YFC0202000: Task 3). R.Z. acknowledges support by the Ministry of Science and Technology of China with Award 2013CB955800, a collaborative research program by Texas A&M University and the National Natural Science Foundation of China, and the Robert A. Welch Foundation (A-1417). W.M.O. acknowledges the support by Luis Strokes Alliance for Minority Participation – Bridge to Doctorate and a National Science Foundation Graduate Research Fellowship Program (GRFP) Fellowship.

References

Chang, D., Song, Y., and Liu, B.: Visibility trends in six megacities in China 1973–2007, Atmos. Res., 94(2), 161-167, 2009.

Chang, R. W., Slowik, J. G., Shantz, N. C., Vlasenko, A., Liggio, J., Sjostedt, S. J., ... and Abbatt, J. P. D.: The hygroscopicity parameter (κ) of ambient organic aerosol at a field site subject to biogenic and anthropogenic influences: relationship to degree of aerosol oxidation, Atmos. Chem. Phys., 10(11), 5047-5064, 2010.

Geller, M., Biswas, S., and Sioutas, C.: Determination of particle effective density in urban environments with a differential mobility analyzer and aerosol particle mass analyzer, Aerosol Sci. Tech., 40(9), 709-723. doi: 10.1080/02786820600803925, 2006.

Guo, S., Hu, M., Zamora, M. L., Peng, J. F., Shang, D. J., Zheng, J., Du, Z. F., Wu, Z., Shao, M., Zeng, L. M., Molina, M. J., and Zhang, R. Y.: Elucidating severe urban haze formation in China, P. Natl. Acad. Sci. U.S.A., 111, 17373-17378, doi:10.1073/pnas.1419604111, 2014.

Hennigan, C.J., Sullivan, A.P., Fountoukis, C.I., Nenes, A., Hecobian, A., Vargas, O., Peltier, R.E., Case Hanks, A.T., Huey, L.G., Lefer, B.L., and Russell, A.G.: On the volatility and production mechanisms of newly formed nitrate and water soluble organic aerosol in Mexico City, Atmos. Chem. Phys., 8(14), 3761-3768, 2008.

Huang, R.-J., Zhang, Y., Bozzetti, C., Ho, K.-F., Cao, J.-J., Han, Y., Daellenbach, K. R., Slowik, J. G., Platt, S. M., Canonaco, F., Zotter, P., Wolf, R., Pieber, S. M., Bruns, E. A., Crippa, M., Ciarelli, G., Piazzalunga, A., Schwikowski, M., Abbaszade, G., Schnelle-Kreis, J., Zimmermann, R., An, Z., Szidat, S., Baltensperger, U., Haddad, I. E., and Prévôt, A. S. H.: High secondary aerosol contribution to particulate pollution during haze events in China, Nature, 514(7521), 218-222, doi:10.1038/nature13774, 2014.

Huang, X. F., He, L. Y., Hu, M., Canagaratna, M. R., Sun, Y., Zhang, Q., Zhu, T., Xue, L., Zeng, L. W., Liu, X. G., Zhang, Y. H., Jayne, J. T., Ng, N. L., and Worsnop, D. R.: Highly time-resolved chemical characterization of atmospheric submicron particles during 2008 Beijing Olympic Games using an Aerodyne High-Resolution Aerosol Mass Spectrometer, Atmos. Chem. Phys., 10, 8933-8945, doi:10.5194/acp-10-8933-2010, 2010.

Hu, M., Peng, J., Sun, K., Yue, D., Guo, S., Wiedensohler, A., and Wu, Z.: Estimation of Size-Resolved Ambient Particle Density Based on the Measurement of Aerosol Number, Mass, and Chemical Size Distributions in the Winter in Beijing, Environ. Sci. Technol., 120830075118007, doi:10.1021/es204073t, 2012.

Hu, W., Hu, M., Hu, W., Jimenez, J. L., Yuan, B., Chen, W., Wang, M., Wu, Y., Chen, C., Wang, Z., Peng, J., Zeng, L., and Shao, M.: Chemical composition, sources and aging process of sub-micron aerosols in Beijing: contrast between summer and winter, J. Geophys. Res.-Atmos., 121, 1955-1977, doi:10.1002/2015JD024020, 2016.

Khalizov, A. F., Zhang, R., Zhang, D., Xue, H., Pagels, J., and McMurry, P. H.: Formation of highly hygroscopic soot aerosols upon internal mixing with sulfuric acid vapor. J. Geophys. Res.-Atmos., 114(D5). doi: 10.1029/2008JD010595, 2009.

Levy, M. E., Zhang, R. Y., Zheng, J., Tan, H. B., Wang, Y., Molina, L. T., Takahama, S., Russell, L. M., and Li, G. H.: Measurements of submicron aerosols at the California-Mexico border during the Cal-Mex 2010 field campaign, Atmos. Environ., 88, 308-319, 2014.

Peng, J. F., Hu, M., Guo, S., Du, Z. F., Zheng, J., Shang, D. J., Zamora, M. L., Zeng, L. M., Shao, M., Wu, Y. S., Zheng, J., Wang, Y., Glen, C. R., Collins, D. R., Molina, M. J., and Zhang, R. Y.: Markedly enhanced absorption and direct radiative forcing of black carbon under polluted urban environments, P. Natl. Acad. Sci. U.S.A., 113, 4266-4271, 10.1073/pnas.1602310113, 2016.

Petters, M. D., and Kreidenweis, S. M.: A single parameter representation of hygroscopic growth and cloud condensation nucleus activity, Atmos. Chem. Phys., 7, 1961-1971, 2007.

Qiao, K., Wu, Z. J., Pei, X. Y., Liu, Q. Y., Shang, D. J., Zheng, J., Du, Z. F., Zhu, W. F., Wu, Y. S., Lou, S. R., Guo, S., Chan, C. K., Pathak, R. K., Hallquist, M., and Hu, M.: Size-resolved effective density of submicron particles during summertime in the rural atmosphere of Beijing, China, Journal of Environmental Sciences, 73, 69-77, 2018.

Sun, Y., Jiang, Q., Wang, Z., Fu, P., Li, J., Yang, T., and Yin, Y.: Investigation of the sources and evolution processes of severe haze pollution in Beijing in January 2013, J. Geophys. Res.-Atmos., 119(7), 4380-4398, 2014.

Sun, Y. L., Wang, Z. F., Fu, P. Q., Yang, T., Jiang, Q., Dong, H. B., Li, J., and Jia, J. J.: Aerosol composition, sources and processes during wintertime in Beijing, China, Atmos. Chem. Phys., 13, 4577-4592, doi:10.5194/acp-13-4577-2013, 2013.

Su, S., Xiao, R., Jiang, Z., and Zhang, Y.: Characterizing landscape pattern and ecosystem service value changes for urbanization impacts at an eco-regional scale, Appl. Geogr., 34, 295–305, doi:10.1016/j.apgeog.2011.12.001, 2012.

Turpin, B. J. and Lim, H. J.: Species contributions to PM2. 5 mass concentrations: Revisiting common assumptions for estimating organic mass, Aerosol Sci. Tech., 35(1), 602-610, doi: 10.1080/02786820119445, 2001.

Wang, J. Y., Da, L. J., Song, K., and Li, B. L.: Temporal variations of surface water quality in urban, suburban and rural areas during rapid urbanization in Shanghai, China, Environ. Pollut., 152, 387-393, 2008.

Wang, Z. B., Hu, M., Wu, Z. J., Yue, D. L., He, L. Y., Huang, X. F., Liu, X. G., and Wiedensohler, A.: Long-term measurements of particle number size distributions and the relationships with air mass history and source apportionment in the summer of Beijing, Atmospheric Chemistry and Physics, 13, 10159-10170, 10.5194/acp-13-10159-2013, 2013.

World Health Organization. Regional Office for Europe, & World Health Organization. Air quality guidelines: global update 2005: particulate matter, ozone, nitrogen dioxide, and sulfur dioxide. 2006.

Wu, Z., Hu, M., Lin, P., Liu, S., Wehner, B., and Wiedensohler, A.: Particle number size distribution in the urban atmosphere of Beijing, China, Atmos. Environ., 42, 7967–7980, doi:10.1016/j.atmosenv.2008.06.022, 2008.

Yue, D., Hu, M., Wu, Z., Wang, Z., Guo, S., Wehner, B., Nowak, A., Achtert, P., Wiedensohler, A., Jung, J.: Characteristics of aerosol size distributions and new particle formation in the summer in Beijing, J. Geophys. Res.-Atmos., 114(14): 1159-1171, 2010.

Zheng, J., Hu, M., Peng, J. F., Wu, Z. J., Kumar, P., Li, M. R., Wang, Y. J., and Guo, S.: Spatial distributions and chemical properties of PM2.5 based on 21 field campaigns at 17 sites in China, Chemosphere, 159, 480-487, 2016.

Atmos. Chem. Phys. Discuss., https://doi.org/10.5194/acp-2019-308
Manuscript under review for journal Atmos. Chem. Phys.
Discussion started: 23 May 2019

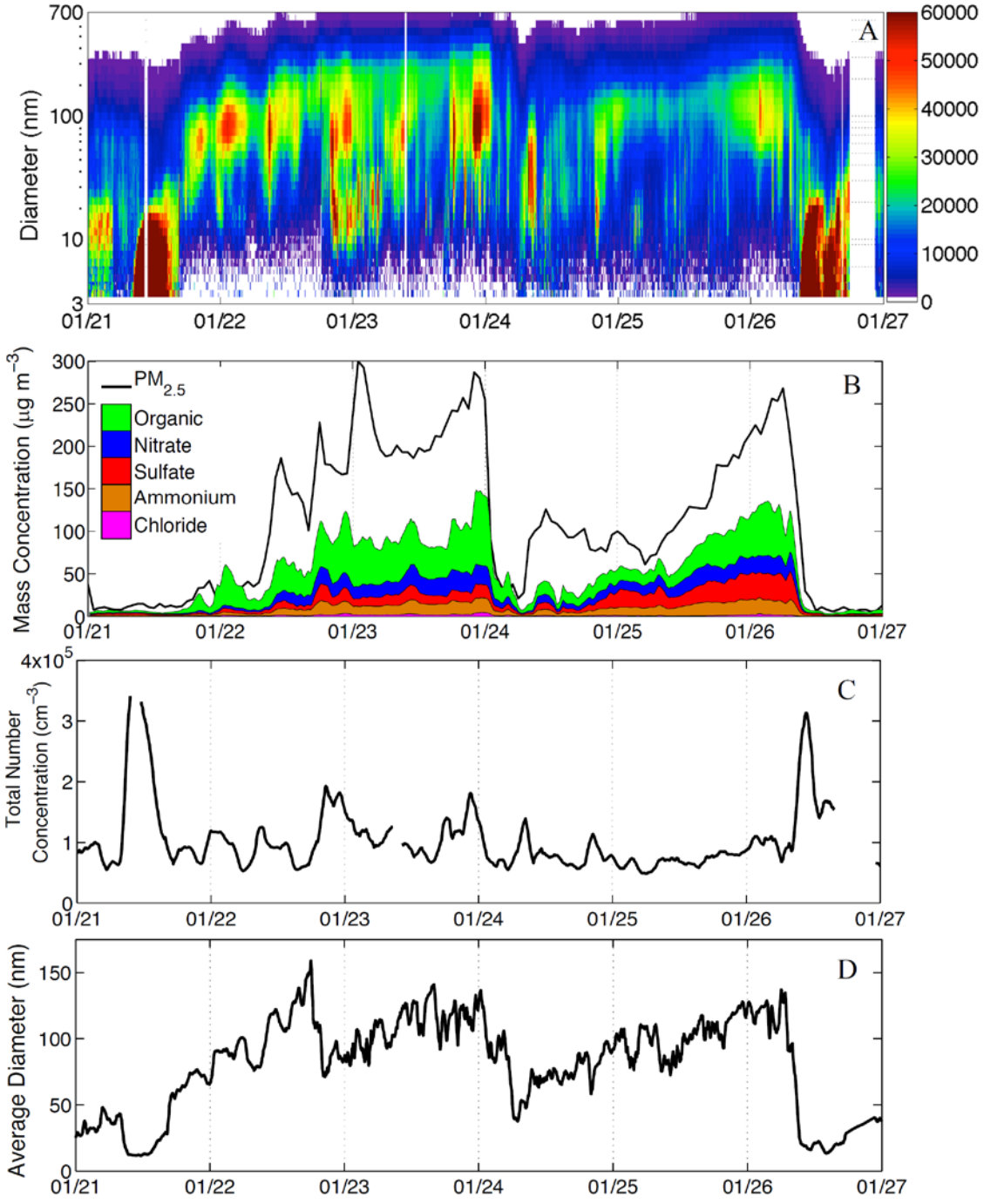

Figure 1. Temporal evolutions of the (A) number size distribution, (B) $PM_{2.5}$ mass concentration, chemical composition, (C) total number concentration, and (D) mean diameter between 21 and 27 January 2015.

Atmos. Chem. Phys. Discuss., https://doi.org/10.5194/acp-2019-308
Manuscript under review for journal Atmos. Chem. Phys.
Discussion started: 23 May 2019

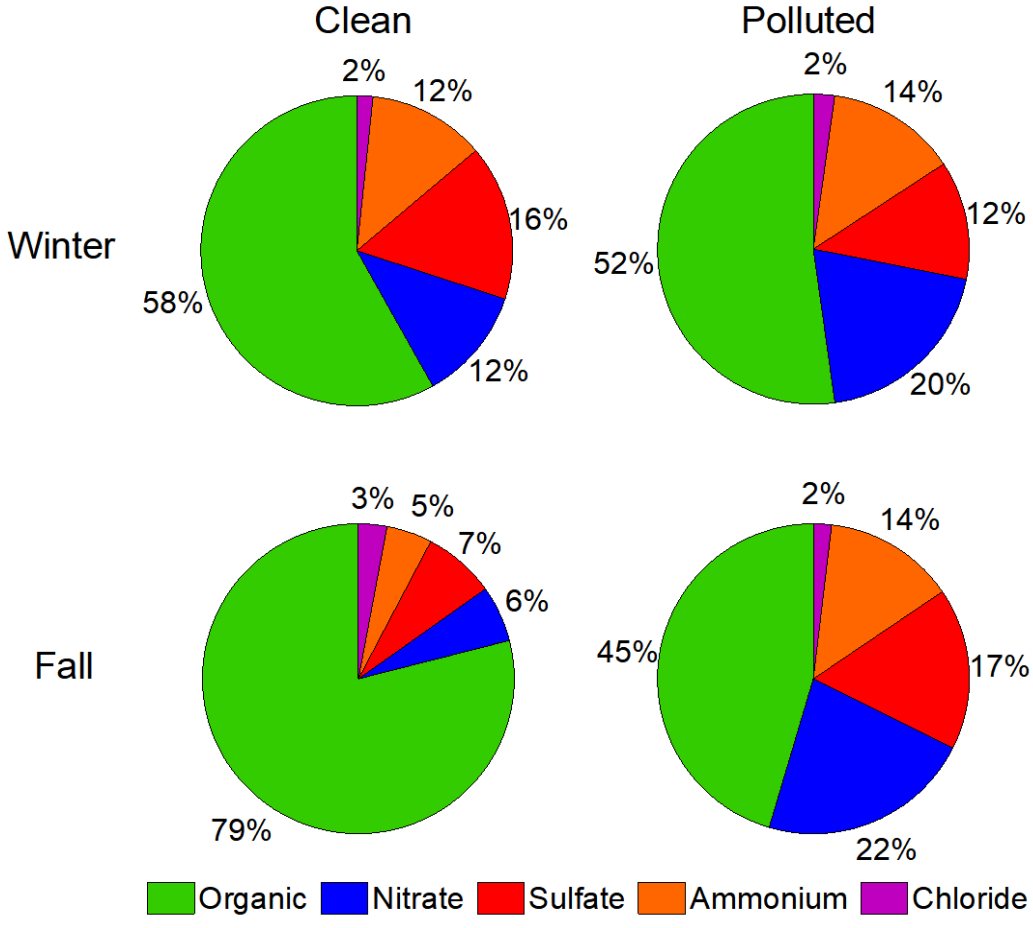

Figure 2. A comparison of the chemical composition during the clean and polluted period from the autumn 2013 and winter 2015 field campaigns.

Atmos. Chem. Phys. Discuss., https://doi.org/10.5194/acp-2019-308
Manuscript under review for journal Atmos. Chem. Phys.
Discussion started: 23 May 2019

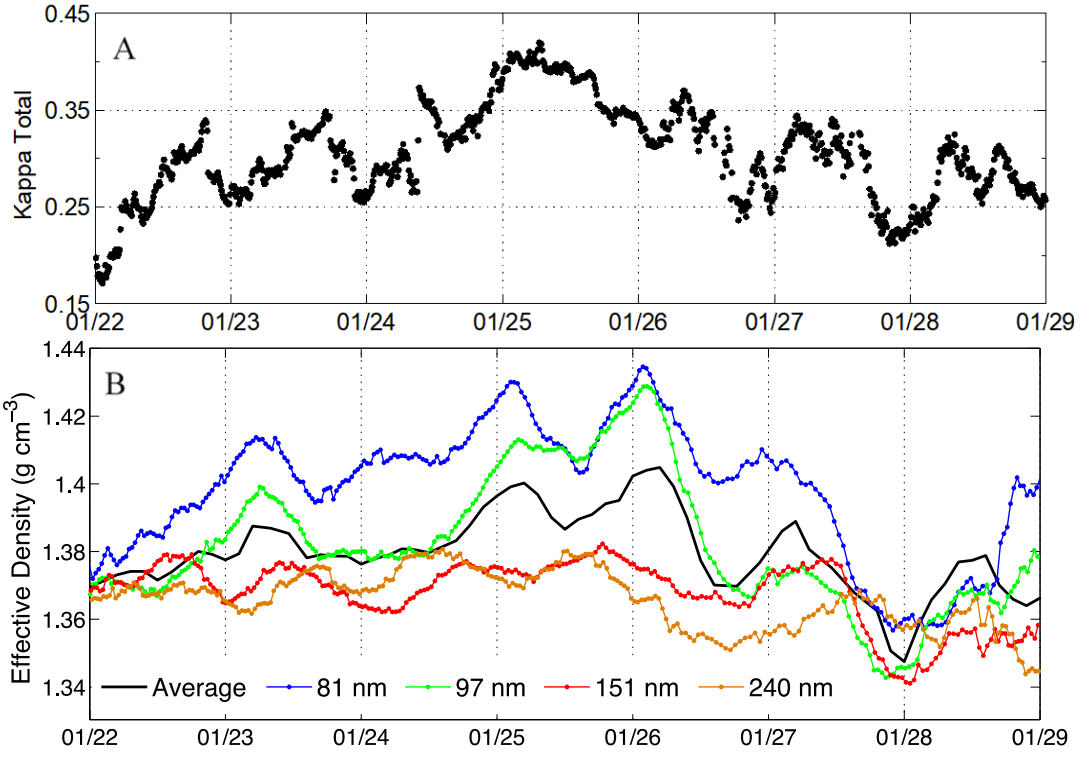

Figure 3. (A) The hygroscopicity determined on the basis of chemical composition (i.e., kappa) of the aerosols. (B) Temporal evolutions of the effective density of particles with a diameter of 81 (blue), 97 (green), 151 (red), 240 nm (orange), and the weighted average of the four particle sizes between 21 and 29 January 2015.

Atmos. Chem. Phys. Discuss., https://doi.org/10.5194/acp-2019-308
Manuscript under review for journal Atmos. Chem. Phys.
Discussion started: 23 May 2019

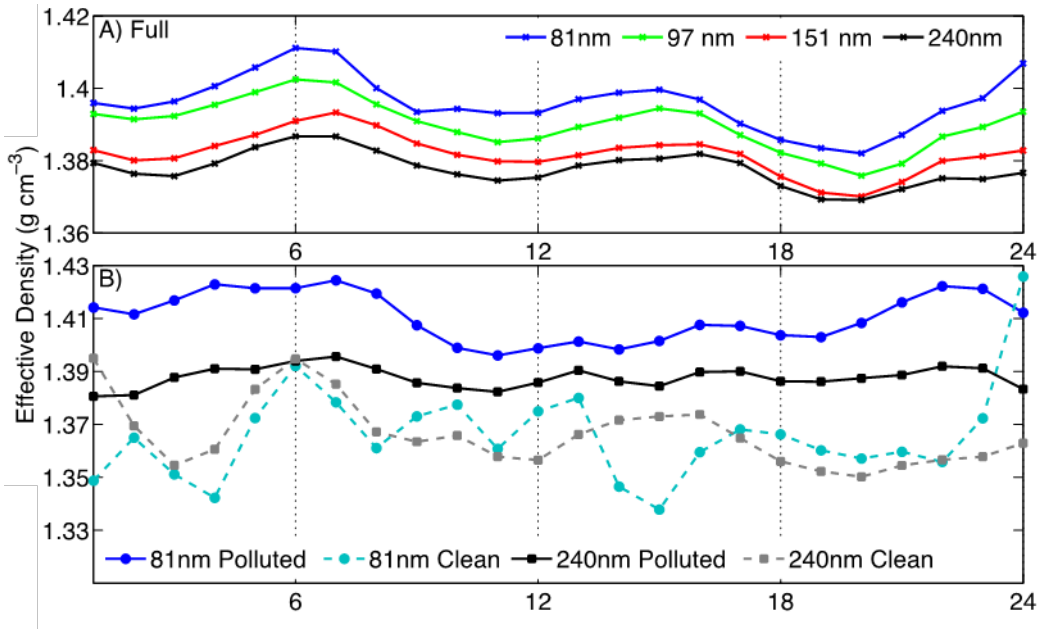

Figure 4. (A) The diurnal variation of the effective density (g cm^{-3}) of the four particle sizes from the full observational period. (B) The effective density (g cm^{-3}) diurnal cycle of the 81 (blue circles) and 240 (black squares) nm particles during the clean (dashed, lighter colors) and polluted periods (solid, darker colors).

Atmos. Chem. Phys. Discuss., https://doi.org/10.5194/acp-2019-308
Manuscript under review for journal Atmos. Chem. Phys.
Discussion started: 23 May 2019

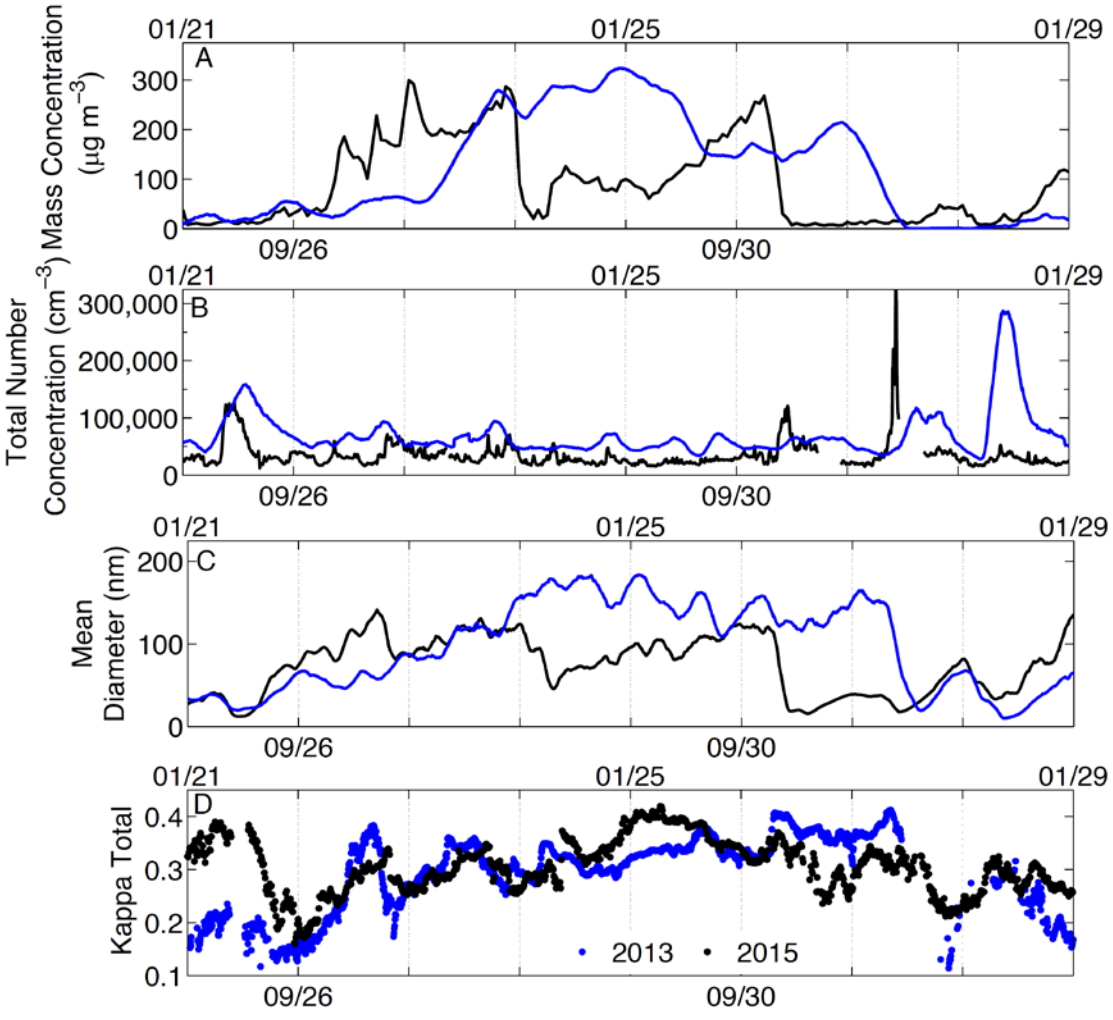

Figure 5. A comparison of the (A) mass concentration, (B) total number concentration, (C) average diameter, and (D) hygroscopicity between the autumn 2013 (blue, bottom axis) and winter 2015 (black, top axis).